NANO LETTERS

pubs.acs.org/NanoLett

Letter

Small-Molecule Therapeutics Achieve Multiple Mechanism-Mediated Sensitizations of Colorectal Cancer to Immune Checkpoint Blockade via Neutrophil Micropharmacies

Xiuqi Li,[§] Xuwentai Liu,[§] Meng Wang,[§] Xinyi Zhang, Ziyao Zhang, Lingjing Xue, Qianqian Xu, Juanjuan Ye, Meixi Hao,* and Can Zhang*

Cite This: *Nano Lett.* 2024, 24, 14531−14540

Read Online

ACCESS | Metrics & More | Article Recommendations | Supporting Information

ABSTRACT: Immune checkpoint blockade (ICB) therapy has been approved for colorectal cancer (CRC). However, response rates are variable and often <50%. The low tumor immunogenicity and immunosuppressive tumor microenvironment (TME) jointly contribute to this suboptimal response rate. This study confirmed the potential of combining immunogenic cell death (ICD) inducer irinotecan (IRI) and transforming growth factor-β (TGF-β) inhibitor galunisertib (GAL) to improve tumor immunogenicity and remodel the immunosuppressive TME. Moreover, to ameliorate the *in vivo* delivery barriers associated with small molecules, neutrophil micropharmacies (NOG) were developed for the codelivery of IRI and GAL, which loaded the commercial liposome formulation of IRI (ONIVYDE, ONI) intracellularly and conjugated the pH-responsive GAL liposome (GLP) on the cell surface. This neutrophil-based formulation resulted in a >4-fold increase in the ratios of the amount of both IRI and GAL accumulated in tumors to the dosage administration, effectively achieving multiple mechanism-mediated sensitization of CRC to ICB therapy.

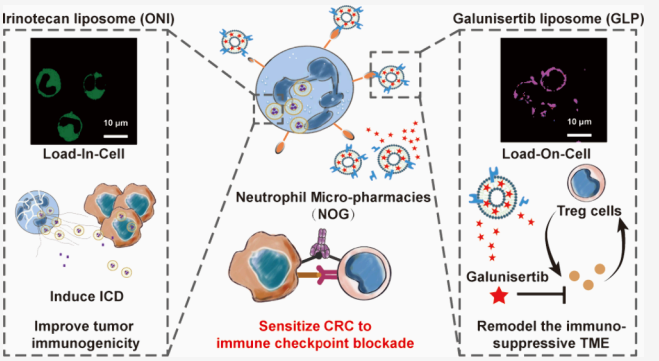

KEYWORDS: *Colorectal cancer, Combination immunotherapy, Immune checkpoint blockade therapy, Neutrophil micropharmacies, Immunogenic cell death, Transforming growth factor-beta inhibitor*

As the third most commonly diagnosed malignancy and the second leading cause of cancer-related death,[1−3] colorectal cancer (CRC) poses a great health threat and urgently requires effective and safe treatments. In recent decades, immune checkpoint blockade (ICB) therapy, represented by targeting the programmed death 1 (PD-1)/programmed death-ligand 1 (PD-L1) pathway, has achieved remarkable progress in the treatment of solid tumors.[4,5] Until now, several PD-1 inhibitors, such as pembrolizumab and nivolumab, have received regulatory approval for CRC treatment.[6,7] Clinical trial data revealed that the objective response rate (ORR) of PD-1 inhibitor monotherapy in CRC is approximately 30−40%, and over 20% of the patients with the best response with pembrolizumab or nivolumab still developed progressive disease.[8,9] Therefore, substantial room for improvement remains, emphasizing the need to explore new strategies to improve the response of CRC to ICB therapy.

Tumor immunogenicity is the fundamental determinant of response to immune checkpoint inhibitors (ICIs) in CRC patients.[10,11] An analysis of the response data for 22 patients with CRC treated with PD-1/PD-L1 inhibitors revealed that cases with low levels of tumor immunogenicity were less responsive to ICIs and more prone to disease progression.[12] Inducing immunogenic cell death (ICD) in cancer cells has been reported to be a viable strategy to improve tumor immunogenicity.[13,14] ICD is characterized as immunogenic apoptosis that activates damage-associated molecular patterns (DAMPs) in dying or dead tumor cells in response to a certain stimulus. DAMPs act as danger signals that activate dendritic cells (DCs) for the presentation of tumor-associated antigens (TAAs), subsequently eliciting T cell-mediated immunological responses against living tumor cells of the same kind.[15,16] Irinotecan (IRI), as a front-line chemotherapy drug for the clinical treatment of CRC,[17] has been reported to trigger ICD in tumors and prolong the overall survival of CRC patients to some extent.[18,19] Overall, IRI is expected to create an exceedingly immunogenic environment and sensitize the CRC to ICB therapy. Furthermore, the complexity of the

Received: August 13, 2024
Revised: October 9, 2024
Accepted: October 10, 2024
Published: October 15, 2024

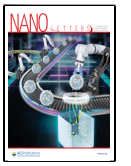

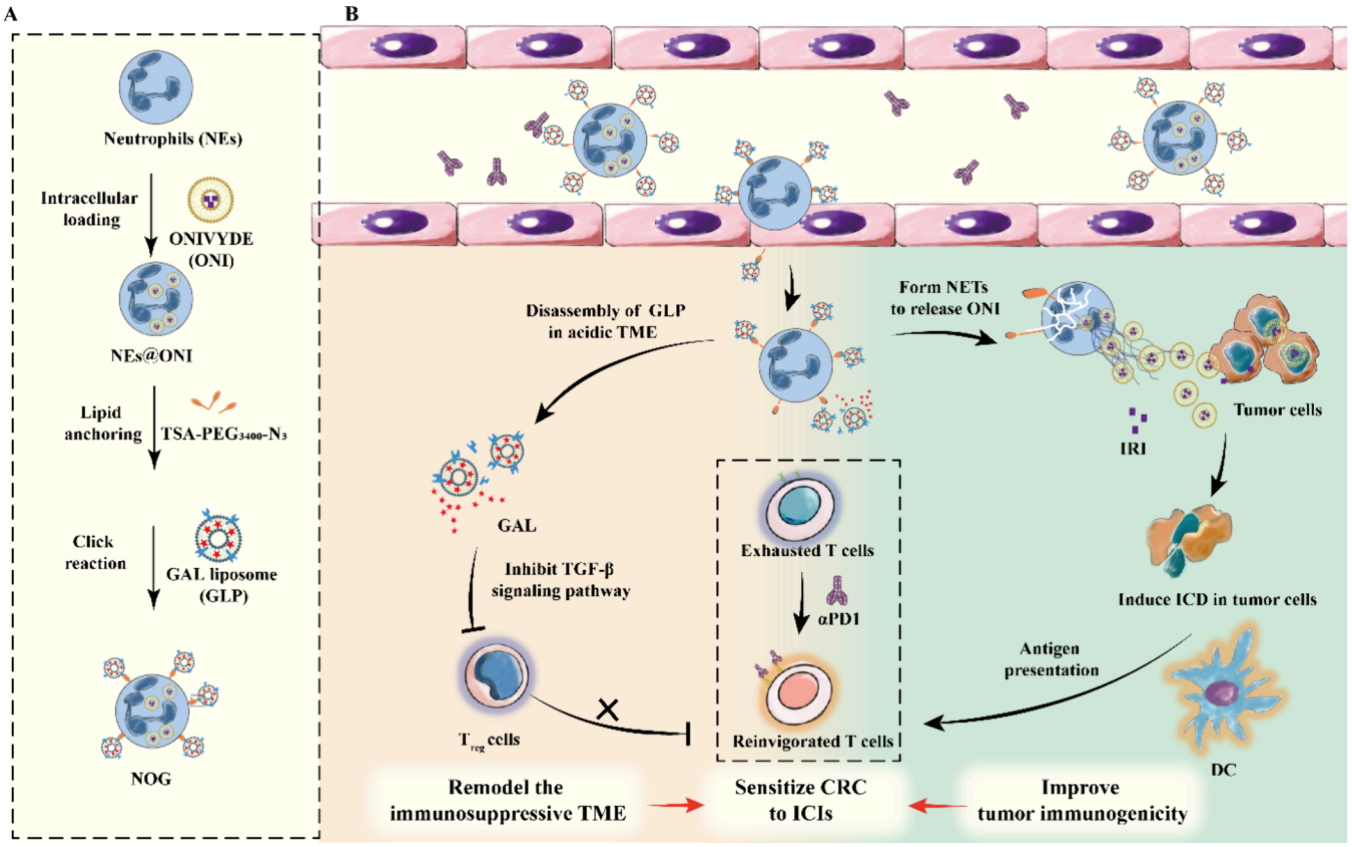

Figure 1. Schematic illustration of IRI and GAL achieving multiple mechanism-mediated sensitization of colorectal cancer to immune checkpoint blockade via neutrophil micropharmacies (NOG). (A) Construction of NOG loaded with ONI intracellularly and conjugated with GLP on the cell surface. (B) The mechanism of action of NOG in sensitizing CRC to ICB therapy and enhancing immunotherapeutic outcomes.

tumor microenvironment (TME) also contributes to the variable response rate to ICB therapy in CRC.[20] Transforming growth factor-beta (TGF-β) is a representative immunosuppressive factor in TME.[21] Recent studies have revealed that after the treatment of ICB, the number of regulatory T cells (Treg) was feedback upregulated and activated, along with the activation of TGF-β signal pathway.[22−24] The activated TGF-β signaling suppresses differentiation and activity of T cells and excludes T cells infiltration into tumors, thereby inducing immune escape in tumors and diminishing the response rate to ICB therapy.[25,26] Thus, the use of TGF-β inhibitors holds promise for reprogramming the immunosuppressive TME and conferring susceptibility to ICB therapy.

Therefore, we supposed that the combination of IRI and TGF-β inhibitor (Galunisertib, GAL) has the potential to improve tumor immunogenicity and remodel the immunosuppressive TME, which confers synergistic immunotherapeutic efficacy to the subsequent ICB therapy and offers therapeutic benefits across a wide spectrum of CRC patients. However, the *in vivo* delivery barriers impede the trafficking of IRI and GAL in the form of free drugs or conventional nanomedicines. The nontumor-targeting systemic distribution of IRI and GAL may lead to inadequate drug accumulation in tumors and potentially severe hematological or cardiac toxicity, respectively.[17,27,28] Thus, it is necessary to develop novel drug delivery carriers and combination strategies to overcome *in vivo* delivery barriers and enhance tumor-targeting efficiency.

Neutrophils (NEs) constitute the largest proportion of leukocyte in peripheral blood.[29−31] As endogenous cells, NEs possess innate ability for physiological barriers traversal through self-deformation.[31,32] Meanwhile, NEs exhibit rapid inflammatory responsiveness, and express the chemokine receptors which facilitate the migration into tumors by binding to various chemokines enriched in tumor lesions, including CXCL1, CXCL2, CXCL5.[33] The pathological analysis of preclinical mouse models of CRC and clinical patients suggested that neutrophils efficiently targeted and infiltrated the CRC tumors.[34,35] In addition, our group has employed NEs as carriers to deliver various nanomedicines and achieve efficient drug delivery and superior efficacy in other solid tumors, such as glioma, hepatoma, gastric cancer and triple-negative breast cancer.[36−40] Therefore, NEs might be a promising carrier to deliver IRI and TGF-β inhibitors targeting CRC.

To maximize the synergistic effects of IRI and GAL, we designed and constructed neutrophil micropharmacies (NOG) using NEs as the codelivery carriers. Briefly, the commercial liposome formulation of IRI (ONIVYDE, ONI)[41] was encapsulated within NEs through phagocytosis. Then, the pH-responsive liposomes loaded with the TGF-β inhibitor (GAL Liposome, GLP) were conjugated onto the surface of NEs@ONI using a two-step method to obtain NOG. The two-step method includes lipid anchoring and click reaction as follows. An azide-bearing lipid (TSA-PEG3400-N_3) was anchored into the lipid bilayer of cells via lipid anchoring, followed by the click reaction between azide and dibenzocyclooctyne (DBCO) modified onto the constitutive lipid of GLP (Figure 1A). The neutrophil micropharmacies exploited the tumor-targeting ability of NEs, facilitating the codelivery of both IRI and GAL to CRC. GAL was released from the pH-

https://doi.org/10.1021/acs.nanolett.4c03678
Nano Lett. 2024, 24, 14531−14540

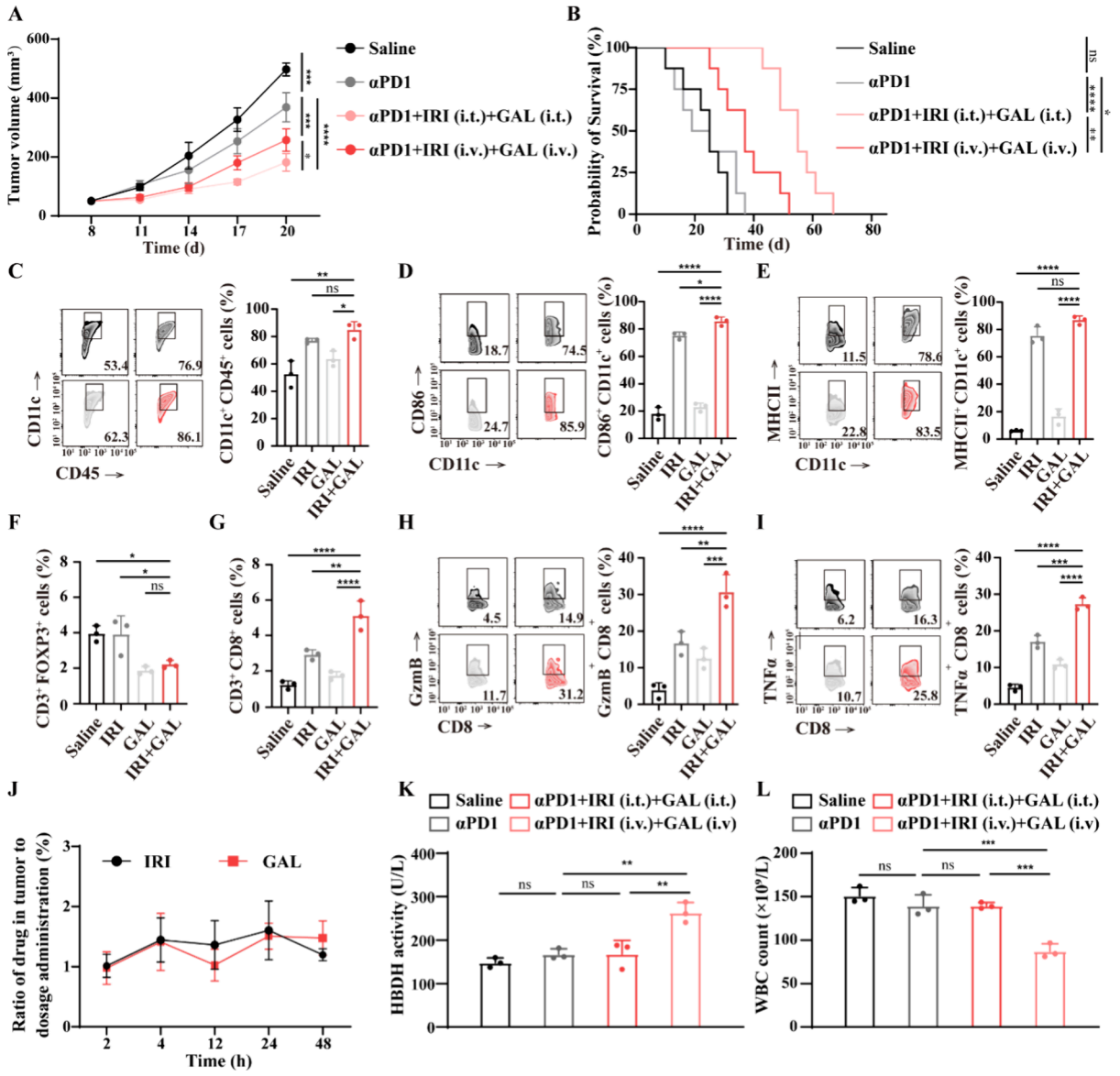

Figure 2. Synergistic effects of IRI and GAL to sensitize ICIs. (A) Tumor volume of MC-38 tumor-bearing mice receiving different treatments (n = 5 mice/group). *i.t.*, intratumoral; *i.v.*, intravenous. (B) Survival curves of mice receiving different treatments (n = 8 mice/group). (C−E) Tumors were isolated after different treatments, and the percentage of dendritic cells (DCs) in tumor infiltrating immune cells (C) and DCs maturation (D and E) were analyzed by flow cytometry. (F,G) Flow cytometry analysis of the percentage of Treg cells ($CD3^+FOXP3^+$). (F) $CD8^+$T cells (G) in $CD8^+$ cells isolated from xenograft MC-38-bearing mice after different treatments. (H,I) Flow cytometry analysis of the function of tumor-infiltrating $CD8^+$ T cells to secret cytokine GzmB (H) and TNFα (I). (J) The ratio of the amount of drug accumulated in tumor to the dosage administration. (K,L) Serum HBDH levels (K) and WBC counts (L) in MC-38-bearing mice receiving different treatments. Data are represented as mean ± SEM and analyzed by student's t test in A or a log-rank (Mantel-Cox) test in B or one-way ANOVA with Tukey's correction in C, D, E, F, G, H, I, K, and L. ns, not significant, $^*P < 0.05$, $^{**}P < 0.01$, $^{***}P < 0.001$, $^{****}P < 0.0001$.

responsive liposome in the acidic TME, inhibiting the activation of the TGF-β signal pathway, thereby preventing the feedback upregulation and activation of Treg cells induced by ICB therapy and activating the immune microenvironment. Moreover, ONI encapsulated in NEs was released via the form of neutrophil extracellular traps (NETs), which were then internalized by tumor cells to induce ICD, promoting antigen presentation, improving tumor immunogenicity, further activating the immune microenvironment, thereby sensitizing ICIs (Figure 1B).

In this study, we propose a new paradigm for codelivery through neutrophils, combining two small-molecule therapeutic agents in a micropharmacy format. Moreover, the combination effect of the TGF-β inhibitor and IRI to remodel the immunosuppressive TME and enhance the response rate of ICB therapy was thoroughly confirmed. Thus, we explore a novel multimechanistic method to synergistically sensitize ICB therapy, which has great clinical potential.

Given our hypothesis that the combination of IRI and GAL is expected to improve tumor immunogenicity and synergistically remodel the immunosuppressive TME, thereby sensitizing ICIs, we first investigated the synergistic effects of IRI and GAL with xenograft CRC-bearing mouse models. The results suggested that the combination of IRI and GAL significantly enhanced the effects of programmed death-1 antibody (αPD1) in delaying tumor progression and prolonged the overall

https://doi.org/10.1021/acs.nanolett.4c03678
Nano Lett. 2024, 24, 14531−14540

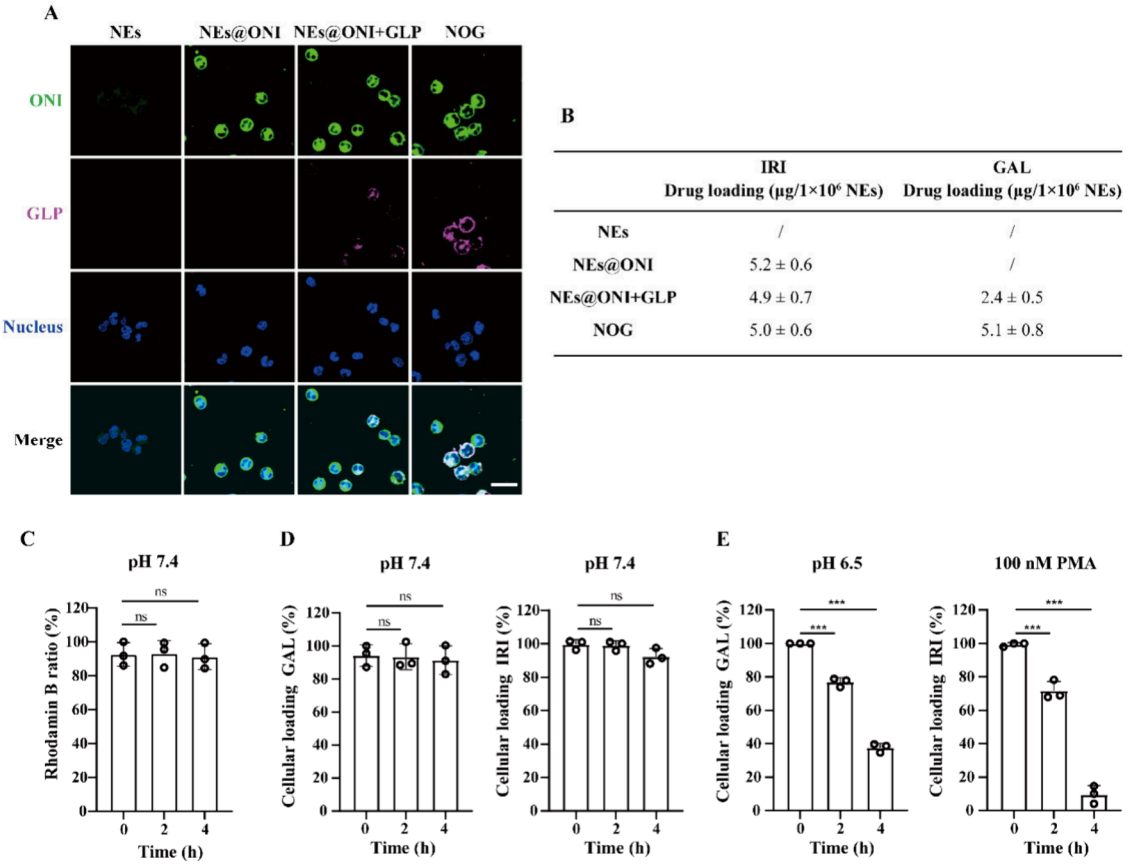

	IRI Drug loading (μg/1×10⁶ NEs)	GAL Drug loading (μg/1×10⁶ NEs)
NEs	/	/
NEs@ONI	5.2 ± 0.6	/
NEs@ONI+GLP	4.9 ± 0.7	2.4 ± 0.5
NOG	5.0 ± 0.6	5.1 ± 0.8

Figure 3. Successful construction and characterization of NOG. (A) Confocal images of NOG. Coumarin 6-labeled ONI (green), rhodamine B-labeled GLP (purple), and cell nucleus (blue). Scale bar, 20 μm. (B) Drug loading of NOG and other control groups. (C) The surface-anchored stability of NOG within 4 h. (D) The GAL-loading stability and IRI-loading stability of NOG within 4 h. (E) Drug release profiles of NOG in the stimulated TME. Data are represented as mean ± SEM and analyzed by one-way ANOVA with Tukey's correction. ns, not significant, ***P < 0.001.

survival of tumor-bearing mice compared to αPD1 monotherapy (Figure 2A and B).

Next, we explored the synergistic mechanism of the combination of IRI and GAL to sensitize αPD1. As presented in Figure S1, treatment with IRI alone or in combination with GAL resulted in an obvious membrane exposure of calreticulin (CRT), increased the secretion of high-mobility group box 1 (HMGB1) in MC-38 cells, and rendered the fragments of dying tumor cells more susceptible to phagocytosis by bone-marrow-derived dendritic cells (BMDCs). The subsequent *in vivo* experiment revealed that the administration of IRI alone or in combination with GAL increased the cell count (Figure 2C), maturation rate (Figure 2D), and antigen presentation capability of tumor infiltrating dendritic cells (Figure 2E). These experiments confirmed that IRI combined with GAL could induce ICD and enhance the tumor immunogenicity. The treatment with GAL alone or in combination with IRI downregulated the expression of TGF-β and the immunosuppressive factors interleukin-10 (IL-10) and interleukin-35 (IL-35) in Treg cells pretreated with αPD1 (Figure S2). The inhibition of Treg cell activation decreased the accumulation of Treg cells at the tumor site, indicating a successful attenuation of the immunosuppressive TME (Figure 2F). Notably, the combined administration of IRI and GAL significantly promoted the infiltration and proliferation of $CD8^+$T cells in tumors (Figure 2G and Figure S3), as well as their secretion of tumor-killing cytokines, including granzyme B (GzmB), and tumor necrosis factor α (TNFα; Figure 2H and I). This promotion effect can be attributed to the synergy of improved tumor immunogenicity via IRI and remodeling of the immunosuppressive TME via GAL.

In addition, we found that the combination of IRI and GAL via intratumoral (*i.t.*) administration was more therapeutically effective than via intravenous (*i.v.*) administration (Figure 2A and B). This may be due to the incomplete distribution of free IRI and GAL in tumors *via i.v.* administration, both accounting for merely 1.9% of the dosage administration (Figure 2J). Moreover, the *i.v.* administration caused elevated plasma α-hydroxybutyrate dehydrogenase (HBDH) levels and a noticeable decrease in white blood cell (WBC) counts in mice, suggesting the potential severe cardiac and hematological toxicities associated with this combination strategy. In contrast, the *i.t.* administration of IRI and GAL displayed negligible cardiac and hematological toxicity (Figure 2K and L). Nevertheless, the complexity of the operation of *i.t.* administration limits its clinical application. Thus, it is necessary to develop novel combination strategies that ensure both safety and effectiveness.

Here, we developed neutrophil micropharmacies (NOG) as a two-drug (IRI and GAL) combination strategy for the treatment of CRC, which possess both safety and effectiveness. To start, we optimized the conditions for encapsulating the ONI into NEs. When ONI was coincubated with NEs at a concentration of 100 μg/mL of IRI for 40 min, the drug

https://doi.org/10.1021/acs.nanolett.4c03678
Nano Lett. 2024, 24, 14531−14540

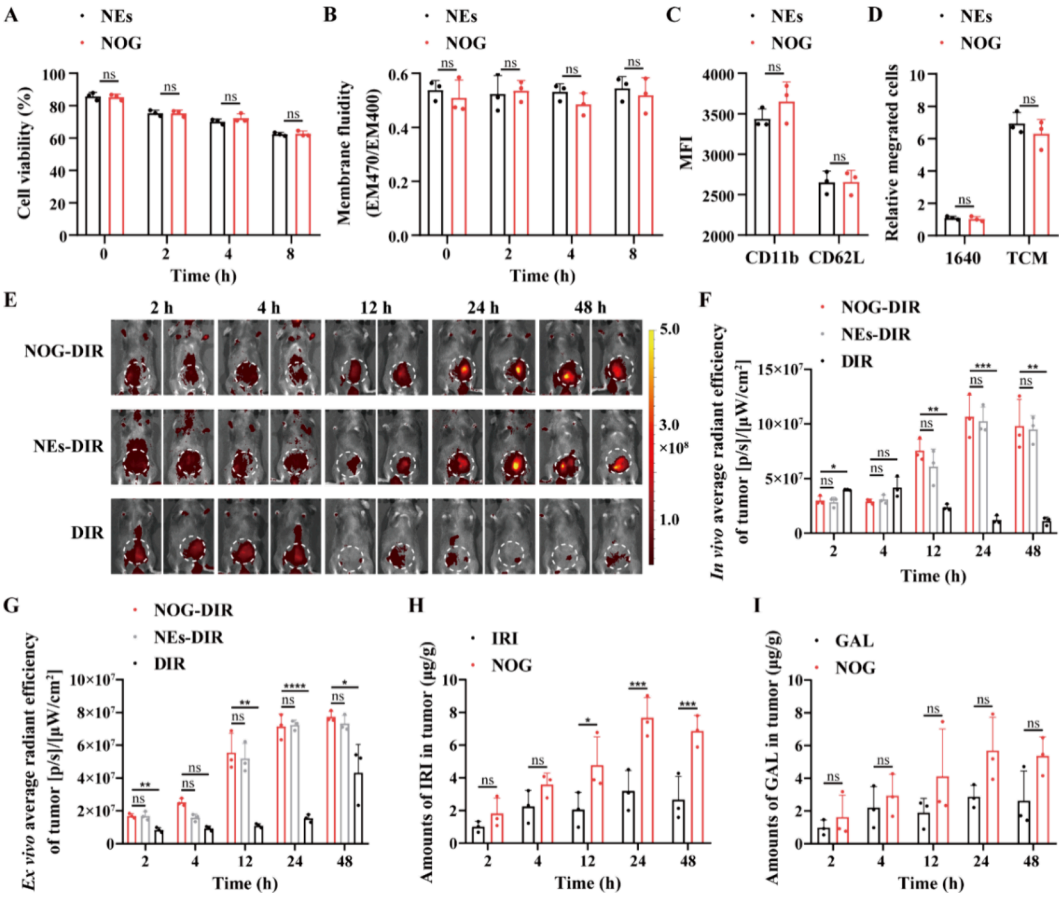

Figure 4. Codelivery of IRI and GAL via NOG. (A) Cell viability of NEs and NOG. (B) Examination of membrane fluidity of NEs and NOG using lipophilic pyrene probes. (C) Flow cytometry analysis of the expression of membrane proteins CD11b and CD62L on NEs and NOG. (D) Quantification of relative migration of NEs and NOG through transwell migration assay. (E,F) *In vivo* imaging (E) and quantification of DIR fluorescence in MC-38-bearing mice receiving DIR, NEs-DIR, and NOG-DIR over time. (G) *Ex vivo* quantification of DIR fluorescence from tumors isolated from MC-38-bearing mice receiving DIR, NEs-DIR, and NOG-DIR over time. (H–I) The concentration of IRI (H) and GAL (I) accumulated in tumors over time after the administration of NOG or free IRI and GAL. Data are represented as mean ± SEM and analyzed by one-way ANOVA with Tukey's correction. ns, not significant, $*P < 0.05$, $**P < 0.01$, $***P < 0.001$, $****P < 0.0001$.

loading peaked at approximately 5.0 μg of IRI per 1 million cells, while cell viability remained above 80% (Figure S4). Moreover, there was no significant impact on the migration and chemotaxis abilities of neutrophils (Figure S5).

Next, for the preparation of GAL-loaded pH-responsive liposome (GLP), the lipid (Chol-NH-DBCO) containing click group-DBCO and pH-responsive group imine was synthesized, and its structure was confirmed by proton nuclear magnetic resonance (^{1}H NMR) and high-resolution mass spectrometry (HRMS, Figure S6). Then, GLP was prepared through the film dispersion method. The obtained GLP showed an average particle size of 155.8 nm and a positive charge of 9.01 mV. The drug loading efficiency (DL%) and entrapment efficiency (EE %) of GAL in GLP were 4.78% and 89.86%, respectively (Figure S7A,B). Representative transmission electron microscopy (TEM) images showed that GLP had a uniform spheroid morphology (Figure S7C).

Subsequently, we conjugated GLP to NEs@ONI using a two-step approach involving lipid anchoring and a click reaction. The click reaction group azide (N_3) was introduced to the cell surface by coincubating NEs@ONI with membrane-anchoring lipid (100 μM, TSA-PEG3400-N_3, Figure S8) for 10 min. Then, the screening of the click reaction conditions between azide on the cell surface and DBCO on the GLP surface revealed a peak amount of drug anchored on NEs@ONI (5.1 μg/1 × 10^6 cells) when the concentration of GLP was set at 200 μg/mL GAL and the incubation time was 30 min (Figure S9). Meanwhile, cell viability remained within an acceptable range (>80%), and the migration and chemotaxis abilities of NEs were also maintained (Figure S10). Eventually, NOG was constructed with ONI located intracellularly and GLP anchored on the surface of NEs. Confocal laser scanning microscopy (CLSM) images revealed that the green fluorescence of coumarin 6 (C6)-labeled ONI was localized intracellularly in NEs, and the deep red fluorescence of rhodamine B-labeled GLP was explicitly localized on the cell membrane (Figure 3A). The results indicate that ONI was firmly confined within the cytoplasm, whereas GLP was successful conjugated onto the cell surface without significant internalization, demonstrating the successful construction of NOG. The final drug loading of NOG was 5.0 μg IRI/1 × 10^6 cells and 5.1 μg GAL/1 × 10^6 cells, respectively (Figure 3B).

Under physiological conditions, neither a significant decrease in the rhodamine B fluorescence intensity of GLP, nor a notable leakage of IRI and GAL was detected within 4 h (Figure 3C and D). These results suggest that NOG possessed good drug loading stability both intracellularly and extracellularly on the cell membrane. In the simulated tumor

https://doi.org/10.1021/acs.nanolett.4c03678
Nano Lett. 2024, 24, 14531−14540

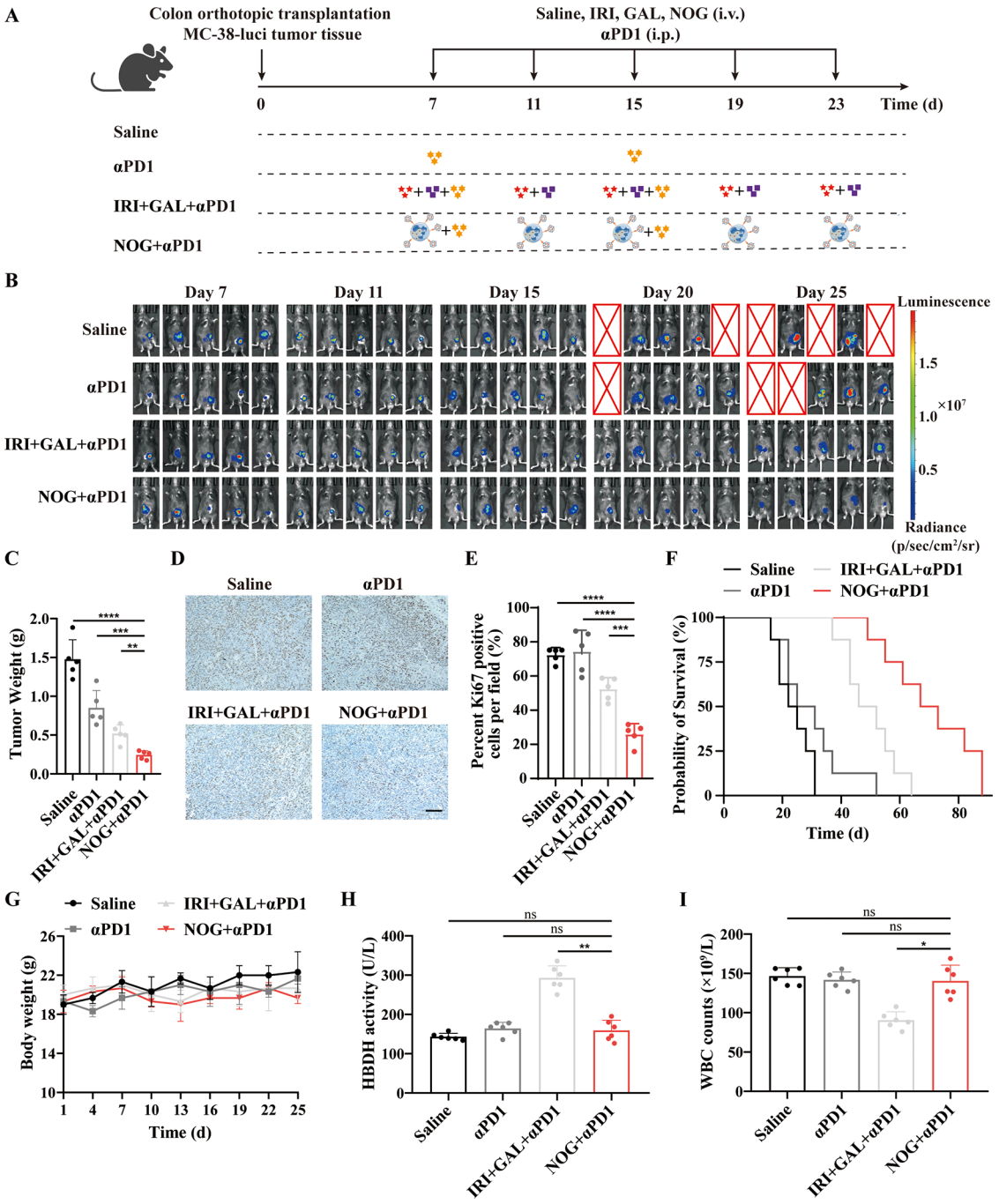

Figure 5. Immune sensitization to αPD1 and safety profile of NOG in the MC-38 orthotopic mouse model. (A) Schematic illustration of the construction of the orthotopic CRC murine model and the design of dosage regimen. (B) *In vivo* bioluminescence images of mice bearing orthotopically transplanted MC-38 tumor cells. (C) Tumor weights of mice receiving different treatments (n = 5 mice/group). (D,E) Representative microscopic images (D) and quantification (E) of tumor sections immuno-stained by Ki67. Ki67 positive areas were quantified from each field (N = 5 fields). Scale bar, 200 μm. (F) Survival curves of mice receiving different treatments (n = 8 mice/group). (G) Body weights of all mice (n = 5 mice/group). (H,I) Serum HBDH levels (H) and WBC counts (I) of tumor-bearing mice receiving different treatments (n = 6 mice/group). Data are represented as mean ± SEM and analyzed by one-way ANOVA with Tukey's correction in C, E, H, and I. ns, not significant, *P < 0.05, **P < 0.01, ***P < 0.001, ****P < 0.0001.

microenvironment, about 60% of GAL was released in the acidic environment (pH = 6.5), whereas more than 90% of IRI was released due to NETs formed by NEs stimulated with 100 nM phorbol myristate acetate (PMA) as described in our pervious report[36] (Figure 3E). This observation suggested that NOG could rapidly release drugs in the simulated tumor microenvironment.

It is essential to preserve the tumor-targeting ability of NOG inherited from NEs to achieve the codelivery of the two drugs to CRC. Therefore, we investigated cell viability, membrane fluidity, chemotaxis-associated protein expression, and tumor chemotaxis, which are associated with tumor-targeting ability of NEs. It was observed that the cell survival rates of both untreated NEs and NOG were over 70% within 8 h, and there was no significant difference between them, suggesting that

https://doi.org/10.1021/acs.nanolett.4c03678
Nano Lett. 2024, 24, 14531−14540

neither the intracellular nor extracellular drug-loading process impaired cell viability (Figure 4A). Moreover, the drug-loading process caused no evident changes in cell membrane fluidity and the expression of critical membrane proteins that mediate cell migration, including CD11b and CD62L (Figure 4B and C). The transwell migration assay revealed that there was no statistically significant difference in the number of cells migrating to the lower chamber between the untreated NEs and the NOG, indicating that the chemotactic ability of NEs remained largely unaffected before and after the drug-loading process (Figure 4D). Additionally, the migration of NOG or NEs to tumor-cell-derived conditioned medium (TCM), which mimicked the CRC microenvironment, was significantly higher than that of RPMI 1640 (Figure 4D). This suggests that NOG could migrate and target the tumor microenvironment of CRC, establishing a basis for further research on the targeted delivery of NOG *in vivo*.

The tumor-targeting capability of NOG *in vivo* was evaluated in orthotopic CRC tumor-bearing mice. We labeled NOG and NEs with 1,1′-dioctadecyl-3,3,3′,3′-tetramethylindotricarbocyanine iodide (DIR) to obtain NOG-DIR and NEs-DIR, and detected their biodistribution by an *in vivo* and *ex vivo* imaging system. NOG exhibited similar dynamics to untreated NEs, as the aggregation of NOG and NEs at the tumor site was observable since 2 h after injection and peaked at 24 h (Figure 4E-G and Figure S11). Meanwhile, the infusion of NOG significantly increased the accumulation of IRI and GAL at the site of CRC. The peak percentages of IRI and GAL in CRC at 24 h were 2-fold and 1.5-fold higher than those in the free drug group (IRI or GAL), respectively (Figure 4H and I).

Moreover, NOG and NEs were mainly distributed in the liver, spleen and lungs after injection, which could be ascribed to the homing ability of NEs to liver and spleen and their retention in the lungs.[42] The distribution of NOG-DIR and NEs-DIR in major organs further confirmed that the drug-loading process did not disturb the *in vivo* distribution of NEs (Figure S12). The biodistribution of IRI and GAL in critical organs was further investigated. The results revealed that NOG significantly reduced the accumulation of GAL in the heart compared to free GAL (Figure S13A). This finding is consistent with the *ex vivo* images of NOG and NEs, neither of which showed a preference for the heart (Figure S12). Taken together, NOG inherits the tumor chemotaxis and tumor-targeting capability of NEs, successfully codelivering the two drugs to the site of CRC.

We next explored whether the NOG could sensitize CRC to αPD1 using an orthotopic CRC murine model. As illustrated in Figure 5A, tumor-bearing mice were treated with *i.v.* administration of free IRI and GAL or NOG, with simultaneous intraperitoneal (*i.p.*) administration of αPD1. The combination therapy of NOG and αPD1 (NOG+αPD1) significantly delayed tumor progression, and its antitumor efficacy was superior to both αPD1 monotherapy and the combination therapy of free drugs plus αPD1 (IRI+GAL +αPD1) (Figure 5B). Meanwhile, tumors in the NOG+αPD1 treated group presented the smallest weight among all of the groups, with a tumor inhibition rate of about 20% (Figure 5C). Moreover, fewer Ki67-positive tumor cells were observed in the NOG+αPD1 treated group (Figure 5D). The number of Ki67-positive cells was half of those in the αPD1 monotherapy group (Figure 5E). The median survival of mice treated with NOG+αPD1 was 70 days, while that of the αPD1 monotherapy group was only 28 days, indicating that NOG combined with αPD1 could significantly extend the median survival of tumor-bearing mice (Figure 5F).

For the safety evaluation, no noticeable reduction in body weight was found in any of the mice during the treatment with different formulations (Figure 5G). However, severe cardiac and hematological toxicities were observed in the mice treated with IRI+GAL+αPD1, which were significantly ameliorated in the NOG combined with the αPD1 treatment group (Figure 5H and I). The reduced cardiac toxicity of GAL is primarily attributed to its reduced distribution in the heart by utilization of NEs as carriers (Figure S12 and Figure S13A). Meanwhile, GAL was loaded into pH-responsive liposomes, designed to release GAL only in acidic environments, such as TME (Figure 3D left and E left). In nonacidic sites, such as the heart, GAL would remain encapsulated, minimizing the risk of cardiac toxicity. Although no significant difference in bone marrow accumulation was observed between free IRI and NOG (Figure S13B), the commercial liposome formulation of IRI (ONI) was encapsulated within NEs, with IRI released via the form of NETs at inflammation sites, such as tumor tissue (Figure 3D right and E right). This ensures IRI release only in areas with inflammatory signals, preventing release in non-inflamed organs, including the bone marrow, where hematological toxicities might otherwise occur. Moreover, IRI is a prodrug, and is activated by human liver carboxylesterase 2 (CES2) to generate SN-38 (7-ethyl-10-hydroxy-camptothecin), the active metabolite that causes cell death. CES activity has been identified in tumors, suggesting localized activation of IRI to the cytotoxic metabolite at the tumor site.[43] Thus, NOG could reduce the distribution of GAL in the liver (Figure S13C), thereby decreasing systemic toxicity from liver-based activation while relying on specific activation at the tumor site.

To mimic the development of CRC in humans and further understand the effect of αPD1 sensitization by NOG, we constructed an orthotopic chemically induced CRC model with the application of carcinogen azoxymethane (AOM) and dextran sodium sulfate (DSS) (Figure S14A). Consistent with the results of the orthotopic CRC model, the NOG+αPD1 treated group displayed the strongest effect of inhibiting tumor progression (Figure S14B and C) and prolonging the survival of tumor-bearing mice (Figure S14D). Moreover, the combination of NOG with αPD1 significantly reduced the activation of the TGF-β signal pathway (Figure S14E and F). Notably, the formulation of NOG also could decrease the severe cardiac and hematological toxicities of free drugs (Figure S14G and H).

Together, these findings further indicate that NOG therapy is safe and effectively increases the response rate of αPD1, possessing the potential to treat CRC patients in clinical settings.

In summary, we developed a novel neutrophil micropharmacy loaded with liposomal IRI intracellularly and conjugated liposomal GAL on the cell membrane surface to achieve the codelivery of both drugs to CRC. This micropharmacy can proactively target CRC due to the physiological barrier-crossing and tumor chemotactic capacity of NEs, resulting in significantly improved tumor accumulation of IRI and GAL. Moreover, the conjugated GAL and loaded IRI were released in response to the stimuli of TME. The released GAL displayed the function of remodeling the immunosuppressive TME, whereas the released IRI was taken up by tumor cells, enhancing tumor immunogenicity by inducing ICD in tumor cells. Our study confirmed the synergistic effect of GAL and

https://doi.org/10.1021/acs.nanolett.4c03678
Nano Lett. 2024, 24, 14531−14540

IRI and demonstrated their role in sensitizing ICB therapy, ultimately achieving a potent antitumor effect against CRC. This study provides a new strategy for optimal combination therapy based on ICB therapy, contributing to exciting therapeutic advancements in cancer immunotherapy.

Statistical Analysis. Statistical analyses were performed using GraphPad Prism 8.0. All plots show mean ± SEM. A one-way ANOVA test was used for comparisons of multiple groups. Student's unpaired *t* test was used for two-group comparisons in the appropriate conditions, and a log-rank (Mantel-Cox) test was used to analyze the statistical significance of difference for survival analysis. Statistical significance was set at $*P < 0.05$, $**P < 0.01$, $***P < 0.001$, and $****P < 0.0001$, ns: no significant difference.

■ ASSOCIATED CONTENT

Supporting Information

The Supporting Information is available free of charge at https://pubs.acs.org/doi/10.1021/acs.nanolett.4c03678.

Detailed materials and methods; Figures S1−S14 of *in vitro* examination of the combination effect of IRI and GAL; the expression of Ki67 in tumor-infiltrating $CD8^+T$ cells; screening of drug loading conditions of NEs@ONI; migration and chemotaxis of NEs@ONI; the synthetic route; ^1H NMR and HRMS spectra of Chol-NH-DBCO; characterization of GLP; the structure and ^1H NMR of TSA-PEG3400-N_3; screening of drug loading conditions of NOG; migration and chemotaxis of NOG; *ex vivo* imaging of DIR in the tumors receiving NOG-DIR, NEs-DIR, and DIR over time; biodistribution evaluation of NOG-DIR, NEs-DIR, and DIR in mice; the accumulation of GAL and IRI in the heart, bone marrow, and liver; and the immune sensitization to αPD1 and safety profile of NOG in the chemically induced CRC model (PDF)

■ AUTHOR INFORMATION

Corresponding Authors

Can Zhang − *State Key Laboratory of Natural Medicines, Center of Advanced Pharmaceuticals and Biomaterials, China Pharmaceutical University, Nanjing 211198, China; Chongqing Innovation Institute of China Pharmaceutical University, Chongqing 401135, China;* orcid.org/0000-0003-3529-5438; Email: zhangcan@cpu.edu.cn

Meixi Hao − *State Key Laboratory of Natural Medicines, Center of Advanced Pharmaceuticals and Biomaterials, China Pharmaceutical University, Nanjing 211198, China; Chongqing Innovation Institute of China Pharmaceutical University, Chongqing 401135, China*; Email: haomeixi@cpu.edu.cn

Authors

Xiuqi Li − *State Key Laboratory of Natural Medicines, Center of Advanced Pharmaceuticals and Biomaterials, China Pharmaceutical University, Nanjing 211198, China; Chongqing Innovation Institute of China Pharmaceutical University, Chongqing 401135, China*

Xuwentai Liu − *State Key Laboratory of Natural Medicines, Center of Advanced Pharmaceuticals and Biomaterials, China Pharmaceutical University, Nanjing 211198, China; Chongqing Innovation Institute of China Pharmaceutical University, Chongqing 401135, China*

Meng Wang − *State Key Laboratory of Natural Medicines, Center of Advanced Pharmaceuticals and Biomaterials, China Pharmaceutical University, Nanjing 211198, China; Chongqing Innovation Institute of China Pharmaceutical University, Chongqing 401135, China*

Xinyi Zhang − *State Key Laboratory of Natural Medicines, Center of Advanced Pharmaceuticals and Biomaterials, China Pharmaceutical University, Nanjing 211198, China; Chongqing Innovation Institute of China Pharmaceutical University, Chongqing 401135, China*

Ziyao Zhang − *State Key Laboratory of Natural Medicines, Center of Advanced Pharmaceuticals and Biomaterials, China Pharmaceutical University, Nanjing 211198, China; Chongqing Innovation Institute of China Pharmaceutical University, Chongqing 401135, China*

Lingjing Xue − *State Key Laboratory of Natural Medicines, Center of Advanced Pharmaceuticals and Biomaterials, China Pharmaceutical University, Nanjing 211198, China; Chongqing Innovation Institute of China Pharmaceutical University, Chongqing 401135, China*

Qianqian Xu − *State Key Laboratory of Natural Medicines, Center of Advanced Pharmaceuticals and Biomaterials, China Pharmaceutical University, Nanjing 211198, China; Chongqing Innovation Institute of China Pharmaceutical University, Chongqing 401135, China*

Juanjuan Ye − *State Key Laboratory of Natural Medicines, Center of Advanced Pharmaceuticals and Biomaterials, China Pharmaceutical University, Nanjing 211198, China; Chongqing Innovation Institute of China Pharmaceutical University, Chongqing 401135, China*

Complete contact information is available at: https://pubs.acs.org/10.1021/acs.nanolett.4c03678

Author Contributions

[§]These authors contributed equally to this work.

Author Contributions

X.L., X.L., and M.W. contributed equally. X.L. conducted most experiments, analyzed the data, and wrote the original manuscript. X.L. designed and conducted most experiments and analyzed the data. M.W. analyzed the data and wrote the manuscript. X.Z. and Z.Z. assisted in most experiments. L.X. assisted in analyzing the data. Q.X. and J.Y. assisted in mice experiments. M.H. supervised all experiments and wrote the manuscript. C.Z. conceived the project and supervised all the experiments.

Notes

The authors declare no competing financial interest.

■ ACKNOWLEDGMENTS

We thank the Public Platform of the State Key Laboratory of Natural Medicines for assistance with imaging of pathological sections. Moreover, we thank Prof. Wenbin Shen and Dr. Huimin Xu of the Public Laboratory Platform at China Pharmaceutical University for assistance with NMR techniques. This work was supported by the National Natural Science Foundation of China (82130102, 92159304, 81930099, 81773664, 82373823, 82104102), the Natural Science Foundation of Jiangsu Province (BK20212011 and BK20230104), Technology innovation project of nucleic acid drug from the National Center of Technology Innovation for Biopharmaceuticals (NCTIB2022HS01014), "Double First-Class" University project (CPU2022QZ05), Project Program

of State Key Laboratory of Natural Medicines (China Pharmaceutical University, SKLNMZZ202310, SKLNMZZ202223), the Fundamental Research Funds for the Central Universities of China (China Pharmaceutical University, 2632023TD01), and Postgraduate Research and Practice Innovation Program of Jiangsu Province (KYCX23_0878).

REFERENCES

(1) Sung, H.; Ferlay, J.; Siegel, R. L.; Laversanne, M.; Soerjomataram, I.; Jemal, A.; Bray, F. Global Cancer Statistics 2020: GLOBOCAN Estimates of Incidence and Mortality Worldwide for 36 Cancers in 185 Countries. *CA Cancer J. Clin* **2021**, *71* (3), 209−249.

(2) Keum, N.; Giovannucci, E. Global Burden of Colorectal Cancer: Emerging Trends, Risk Factors and Prevention Strategies. *Nat. Rev. Gastroenterol Hepatol* **2019**, *16* (12), 713−732.

(3) Dekker, E.; Tanis, P. J.; Vleugels, J. L. A.; Kasi, P. M.; Wallace, M. B. Colorectal Cancer. *Lancet* **2019**, *394* (10207), 1467−1480.

(4) Sharma, P.; Allison, J. P. The Future of Immune Checkpoint Therapy. *Science* **2015**, *348* (6230), 56−61.

(5) Sun, Q.; Hong, Z.; Zhang, C.; Wang, L.; Han, Z.; Ma, D. Immune Checkpoint Therapy for Solid Tumours: Clinical Dilemmas and Future Trends. *Sig Transduct Target Ther* **2023**, *8* (1), 1−26.

(6) Ganesh, K.; Stadler, Z. K.; Cercek, A.; Mendelsohn, R. B.; Shia, J.; Segal, N. H.; Diaz, L. A. Immunotherapy in Colorectal Cancer: Rationale, Challenges and Potential. *Nat. Rev. Gastroenterol Hepatol* **2019**, *16* (6), 361−375.

(7) Casak, S. J.; Marcus, L.; Fashoyin-Aje, L.; Mushti, S. L.; Cheng, J.; Shen, Y.-L.; Pierce, W. F.; Her, L.; Goldberg, K. B.; Theoret, M. R.; Kluetz, P. G.; Pazdur, R.; Lemery, S. J. FDA Approval Summary: Pembrolizumab for the First-Line Treatment of Patients with MSI-H/dMMR Advanced Unresectable or Metastatic Colorectal Carcinoma. *Clin. Cancer Res.* **2021**, *27* (17), 4680−4684.

(8) André, T.; Shiu, K.-K.; Kim, T. W.; Jensen, B. V.; Jensen, L. H.; Punt, C.; Smith, D.; Garcia-Carbonero, R.; Benavides, M.; Gibbs, P.; de la Fouchardiere, C.; Rivera, F.; Elez, E.; Bendell, J.; Le, D. T.; Yoshino, T.; Van Cutsem, E.; Yang, P.; Farooqui, M. Z. H.; Marinello, P.; Diaz, L. A. KEYNOTE-177 Investigators. Pembrolizumab in Microsatellite-Instability-High Advanced Colorectal Cancer. *N Engl J. Med.* **2020**, *383* (23), 2207−2218.

(9) Overman, M. J.; McDermott, R.; Leach, J. L.; Lonardi, S.; Lenz, H.-J.; Morse, M. A.; Desai, J.; Hill, A.; Axelson, M.; Moss, R. A.; Goldberg, M. V.; Cao, Z. A.; Ledeine, J.-M.; Maglinte, G. A.; Kopetz, S.; André, T. Nivolumab in Patients with Metastatic DNA Mismatch Repair-Deficient or Microsatellite Instability-High Colorectal Cancer (CheckMate 142): An Open-Label, Multicentre, Phase 2 Study. *Lancet Oncol* **2017**, *18* (9), 1182−1191.

(10) Yarchoan, M.; Hopkins, A.; Jaffee, E. M. Tumor Mutational Burden and Response Rate to PD-1 Inhibition. *N Engl J. Med.* **2017**, *377* (25), 2500−2501.

(11) Wang, S.; He, Z.; Wang, X.; Li, H.; Liu, X.-S. Antigen Presentation and Tumor Immunogenicity in Cancer Immunotherapy Response Prediction. *eLife* **2019**, *8*, No. e49020.

(12) Schrock, A. B.; Ouyang, C.; Sandhu, J.; Sokol, E.; Jin, D.; Ross, J. S.; Miller, V. A.; Lim, D.; Amanam, I.; Chao, J.; Catenacci, D.; Cho, M.; Braiteh, F.; Klempner, S. J.; Ali, S. M.; Fakih, M. Tumor Mutational Burden Is Predictive of Response to Immune Checkpoint Inhibitors in MSI-High Metastatic Colorectal Cancer. *Annals of Oncology* **2019**, *30* (7), 1096−1103.

(13) Galon, J.; Bruni, D. Approaches to Treat Immune Hot, Altered and Cold Tumours with Combination Immunotherapies. *Nat. Rev. Drug Discov* **2019**, *18* (3), 197−218.

(14) Pfirschke, C.; Engblom, C.; Rickelt, S.; Cortez-Retamozo, V.; Garris, C.; Pucci, F.; Yamazaki, T.; Poirier-Colame, V.; Newton, A.; Redouane, Y.; Lin, Y.-J.; Wojtkiewicz, G.; Iwamoto, Y.; Mino-Kenudson, M.; Huynh, T. G.; Hynes, R. O.; Freeman, G. J.; Kroemer, G.; Zitvogel, L.; Weissleder, R.; Pittet, M. J. Immunogenic Chemotherapy Sensitizes Tumors to Checkpoint Blockade Therapy. *Immunity* **2016**, *44* (2), 343−354.

(15) Krysko, D. V.; Garg, A. D.; Kaczmarek, A.; Krysko, O.; Agostinis, P.; Vandenabeele, P. Immunogenic Cell Death and DAMPs in Cancer Therapy. *Nat. Rev. Cancer* **2012**, *12* (12), 860−875.

(16) Kroemer, G.; Galassi, C.; Zitvogel, L.; Galluzzi, L. Immunogenic Cell Stress and Death. *Nat. Immunol* **2022**, *23* (4), 487−500.

(17) Bailly, C. Irinotecan: 25 Years of Cancer Treatment. *Pharmacol. Res.* **2019**, *148*, 104398.

(18) McKenzie, J. A.; Mbofung, R. M.; Malu, S.; Zhang, M.; Ashkin, E.; Devi, S.; Williams, L.; Tieu, T.; Peng, W.; Pradeep, S.; Xu, C.; Zorro Manrique, S.; Liu, C.; Huang, L.; Chen, Y.; Forget, M.-A.; Haymaker, C.; Bernatchez, C.; Satani, N.; Muller, F.; Roszik, J.; Kalra, A.; Heffernan, T.; Sood, A.; Hu, J.; Amaria, R.; Davis, R. E.; Hwu, P. The Effect of Topoisomerase I Inhibitors on the Efficacy of T-Cell-Based Cancer Immunotherapy. *J. Natl. Cancer Inst* **2018**, *110* (7), 777−786.

(19) Frey, B.; Stache, C.; Rubner, Y.; Werthmöller, N.; Schulz, K.; Sieber, R.; Semrau, S.; Rödel, F.; Fietkau, R.; Gaipl, U. S. Combined Treatment of Human Colorectal Tumor Cell Lines with Chemotherapeutic Agents and Ionizing Irradiation Can in Vitro Induce Tumor Cell Death Forms with Immunogenic Potential. *J. Immunotoxicol* **2012**, *9* (3), 301−313.

(20) Binnewies, M.; Roberts, E. W.; Kersten, K.; Chan, V.; Fearon, D. F.; Merad, M.; Coussens, L. M.; Gabrilovich, D. I.; Ostrand-Rosenberg, S.; Hedrick, C. C.; Vonderheide, R. H.; Pittet, M. J.; Jain, R. K.; Zou, W.; Howcroft, T. K.; Woodhouse, E. C.; Weinberg, R. A.; Krummel, M. F. Understanding the Tumor Immune Microenvironment (TIME) for Effective Therapy. *Nat. Med.* **2018**, *24* (5), 541−550.

(21) Massagué, J.; Blain, S. W.; Lo, R. S. TGFbeta Signaling in Growth Control, Cancer, and Heritable Disorders. *Cell* **2000**, *103* (2), 295−309.

(22) Maj, T.; Wang, W.; Crespo, J.; Zhang, H.; Wang, W.; Wei, S.; Zhao, L.; Vatan, L.; Shao, I.; Szeliga, W.; Lyssiotis, C.; Liu, J. R.; Kryczek, I.; Zou, W. Oxidative Stress Controls Regulatory T Cell Apoptosis and Suppressor Activity and PD-L1-Blockade Resistance in Tumor. *Nat. Immunol* **2017**, *18* (12), 1332−1341.

(23) Zheng, Y.; Josefowicz, S.; Chaudhry, A.; Peng, X. P.; Forbush, K.; Rudensky, A. Y. Role of Conserved Non-Coding DNA Elements in the Foxp3 Gene in Regulatory T-Cell Fate. *Nature* **2010**, *463* (7282), 808−812.

(24) Worthington, J. J.; Kelly, A.; Smedley, C.; Bauché, D.; Campbell, S.; Marie, J. C.; Travis, M. A. Integrin Avβ8-Mediated TGF-β Activation by Effector Regulatory T Cells Is Essential for Suppression of T-Cell-Mediated Inflammation. *Immunity* **2015**, *42* (5), 903−915.

(25) Tauriello, D. V. F.; Palomo-Ponce, S.; Stork, D.; Berenguer-Llergo, A.; Badia-Ramentol, J.; Iglesias, M.; Sevillano, M.; Ibiza, S.; Cañellas, A.; Hernando-Momblona, X.; Byrom, D.; Matarin, J. A.; Calon, A.; Rivas, E. I.; Nebreda, A. R.; Riera, A.; Attolini, C. S.-O.; Batlle, E. TGFβ Drives Immune Evasion in Genetically Reconstituted Colon Cancer Metastasis. *Nature* **2018**, *554* (7693), 538−543.

(26) Mariathasan, S.; Turley, S. J.; Nickles, D.; Castiglioni, A.; Yuen, K.; Wang, Y.; Kadel, E. E.; Koeppen, H.; Astarita, J. L.; Cubas, R.; Jhunjhunwala, S.; Banchereau, R.; Yang, Y.; Guan, Y.; Chalouni, C.; Ziai, J.; Şenbabaoğlu, Y.; Santoro, S.; Sheinson, D.; Hung, J.; Giltnane, J. M.; Pierce, A. A.; Mesh, K.; Lianoglou, S.; Riegler, J.; Carano, R. A. D.; Eriksson, P.; Höglund, M.; Somarriba, L.; Halligan, D. L.; van der Heijden, M. S.; Loriot, Y.; Rosenberg, J. E.; Fong, L.; Mellman, I.; Chen, D. S.; Green, M.; Derleth, C.; Fine, G. D.; Hegde, P. S.; Bourgon, R.; Powles, T. TGFβ Attenuates Tumour Response to PD-L1 Blockade by Contributing to Exclusion of T Cells. *Nature* **2018**, *554* (7693), 544−548.

(27) Credill, K. M.; Stauber, A. J. Nonclinical Safety Evaluation of a Transforming Growth Factor β Receptor I Kinase Inhibitor in Fischer 344 Rats and Beagle Dogs. *J. Clin Toxicol* **2014**, *04* (03), 1−10.

https://doi.org/10.1021/acs.nanolett.4c03678
Nano Lett. 2024, 24, 14531−14540

(28) Cassidy, K. C.; Gueorguieva, I.; Miles, C.; Rehmel, J.; Yi, P.; Ehlhardt, W. J. Disposition and Metabolism of [14C]-Galunisertib, a TGF-βRI Kinase/ALK5 Inhibitor, Following Oral Administration in Healthy Subjects and Mechanistic Prediction of the Effect of Itraconazole on Galunisertib Pharmacokinetics. *Xenobiotica* **2018**, *48* (4), 382−399.
(29) Ballesteros, I.; Rubio-Ponce, A.; Genua, M.; Lusito, E.; Kwok, I.; Fernández-Calvo, G.; Khoyratty, T. E.; van Grinsven, E.; González-Hernández, S.; Nicolás-Ávila, J. Á.; Vicanolo, T.; Maccataio, A.; Benguría, A.; Li, J. L.; Adrover, J. M.; Aroca-Crevillen, A.; Quintana, J. A.; Martín-Salamanca, S.; Mayo, F.; Ascher, S.; Barbiera, G.; Soehnlein, O.; Gunzer, M.; Ginhoux, F.; Sánchez-Cabo, F.; Nistal-Villán, E.; Schulz, C.; Dopazo, A.; Reinhardt, C.; Udalova, I. A.; Ng, L. G.; Ostuni, R.; Hidalgo, A. Co-Option of Neutrophil Fates by Tissue Environments. *Cell* **2020**, *183* (5), 1282−1297.
(30) Németh, T.; Sperandio, M.; Mócsai, A. Neutrophils as Emerging Therapeutic Targets. *Nat. Rev. Drug Discov* **2020**, *19* (4), 253−275.
(31) Kolaczkowska, E.; Kubes, P. Neutrophil Recruitment and Function in Health and Inflammation. *Nat. Rev. Immunol* **2013**, *13* (3), 159−175.
(32) Coffelt, S. B.; Wellenstein, M. D.; de Visser, K. E. Neutrophils in Cancer: Neutral No More. *Nat. Rev. Cancer* **2016**, *16* (7), 431−446.
(33) Jablonska, J.; Wu, C.-F.; Andzinski, L.; Leschner, S.; Weiss, S. CXCR2-Mediated Tumor-Associated Neutrophil Recruitment Is Regulated by IFN-β. *Int. J. Cancer* **2014**, *134* (6), 1346−1358.
(34) Jackstadt, R.; van Hooff, S. R.; Leach, J. D.; Cortes-Lavaud, X.; Lohuis, J. O.; Ridgway, R. A.; Wouters, V. M.; Roper, J.; Kendall, T. J.; Roxburgh, C. S.; Horgan, P. G.; Nixon, C.; Nourse, C.; Gunzer, M.; Clark, W.; Hedley, A.; Yilmaz, O. H.; Rashid, M.; Bailey, P.; Biankin, A. V.; Campbell, A. D.; Adams, D. J.; Barry, S. T.; Steele, C. W.; Medema, J. P.; Sansom, O. J. Epithelial NOTCH Signaling Rewires the Tumor Microenvironment of Colorectal Cancer to Drive Poor-Prognosis Subtypes and Metastasis. *Cancer Cell* **2019**, *36* (3), 319−336.
(35) Klintrup, K.; Mäkinen, J. M.; Kauppila, S.; Väre, P. O.; Melkko, J.; Tuominen, H.; Tuppurainen, K.; Mäkelä, J.; Karttunen, T. J.; Mäkinen, M. J. Inflammation and Prognosis in Colorectal Cancer. *Eur. J. Cancer* **2005**, *41* (17), 2645−2654.
(36) Xue, J.; Zhao, Z.; Zhang, L.; Xue, L.; Shen, S.; Wen, Y.; Wei, Z.; Wang, L.; Kong, L.; Sun, H.; Ping, Q.; Mo, R.; Zhang, C. Neutrophil-Mediated Anticancer Drug Delivery for Suppression of Postoperative Malignant Glioma Recurrence. *Nat. Nanotechnol.* **2017**, *12* (7), 692−700.
(37) Zhang, L.; Zhang, Y.; Xue, Y.; Wu, Y.; Wang, Q.; Xue, L.; Su, Z.; Zhang, C. Transforming Weakness into Strength: Photothermal-Therapy-Induced Inflammation Enhanced Cytopharmaceutical Chemotherapy as a Combination Anticancer Treatment. *Adv. Mater.* **2019**, *31*, 1805936.
(38) Ju, C.; Wen, Y.; Zhang, L.; Wang, Q.; Xue, L.; Shen, J.; Zhang, C. Neoadjuvant Chemotherapy Based on Abraxane/Human Neutrophils Cytopharmaceuticals with Radiotherapy for Gastric Cancer. *Small* **2019**, *15* (5), No. e1804191.
(39) Hao, M.; Zhu, L.; Hou, S.; Chen, S.; Li, X.; Li, K.; Zhu, N.; Chen, S.; Xue, L.; Ju, C.; Zhang, C. Sensitizing Tumors to Immune Checkpoint Blockage via STING Agonists Delivered by Tumor-Penetrating Neutrophil Cytopharmaceuticals. *ACS Nano* **2023**, *17* (2), 1663−1680.
(40) Zhang, L.; Wang, Q.; Dai, Y.; Chen, J.; Wu, T.; Ju, C.; Xue, L.; Zhang, C. New-Generation Cytopharmaceuticals with Powerfully Boosted Extravasation for Enhanced Cancer Therapy. *J. Controlled Release* **2023**, *359*, 116−131.
(41) Zhang, H. Onivyde for the Therapy of Multiple Solid Tumors. *Onco Targets Ther* **2016**, *9*, 3001−3007.
(42) Kumbhojkar, N.; Prakash, S.; Fukuta, T.; Adu-Berchie, K.; Kapate, N.; An, R.; Darko, S.; Chandran Suja, V.; Park, K. S.; Gottlieb, A. P.; Bibbey, M. G.; Mukherji, M.; Wang, L. L.-W.; Mooney, D. J.; Mitragotri, S. Neutrophils Bearing Adhesive Polymer Micropatches as a Drug-Free Cancer Immunotherapy. *Nat. Biomed Eng.* **2024**, *8* (5), 579−592.
(43) Xu, G.; Zhang, W.; Ma, M. K.; McLeod, H. L. Human Carboxylesterase 2 Is Commonly Expressed in Tumor Tissue and Is Correlated with Activation of Irinotecan. *Clin. Cancer Res.* **2002**, *8* (8), 2605−2611.

https://doi.org/10.1021/acs.nanolett.4c03678
Nano Lett. 2024, 24, 14531−14540